Position control of electro-hydraulic servo system using active disturbance rejection control for upper-limb exoskeleton

Jing Tang[1], Jiaxun Cao[2], Minghu Wu[3], Lun Zhao[4], Fan Zhang[5]
[1, 2, 3, 4, 5]School of Electrical and Electronic Engineering, Hubei University of Technology, Wuhan, China
[1, 3, 5]Hubei Collaborative Innovation Center for High-efficiency Utilization of Solar Energy, Hubei University of Technology, Wuhan 430068, China
[3]Corresponding author
E-mail: [1]*mimitang85119@163.com*, [2]*1070161573@qq.com*, [3]*18732463@qq.com*, [4]*allenzhao.he@qq.com*, [5]*joyce_zhang@hbut.edu.cn*

Received 4 August 2022; accepted 24 November 2022; published online 7 January 2023
DOI https://doi.org/10.21595/jve.2022.22850

Abstract. This paper presents a two-degree-of-freedom(2-DOF) upper-limb exoskeleton actuated by electro-hydraulic servo system (EHSS), and position control based on active disturbance rejection control (ADRC) strategy. Proportional integral derivative (PID) controller is widely used in EHSS system because it is model free, and its parameters can be adjusted easily. However, the nonlinear dynamics of EHSS is subject to parameter variations and friction effects during operation. The trajectory tracking performance of this method is limited due to the uncertain model parameter and external disturbance of EHSS in exoskeleton. To actively compensate the total disturbance including the system uncertainty and external disturbance, and ensure the finite time convergence of disturbances, the ADRC controller is developed. The disturbances can be estimated by the extended state observer (ESO) and compensated during each sampling period in the ADRC method. The proposed control strategy not only satisfies the steady-state accuracy demands, but also effectively resists to the system uncertainties and the disturbance. To validate the feasibility of the proposed control strategy, the simulations were carried out. The numerical simulation results clearly indicate the superior performance of proposed ADRC method over the regular PID control approach.

Keywords: two-degree-of-freedom upper-limb exoskeleton, electro-hydraulic servo system, active disturbance rejection control, extend state observer.

1. Introduction

Upper-limb exoskeleton robots are generally applied in a variety of different fields, such as rehabilitation robots [1-3], assistive robots [4-6], human amplifiers [7, 8] and other uses. Robotic exoskeleton is the complex multi-input and multi-output (MIMO) with time varying dynamics and highly coupled nonlinear [9]. Compared with industrial manipulators, exoskeletons suffer severe kinematic and dynamic uncertainties and external disturbances. Electro-hydraulic actuators have been used in exoskeleton in a wide number of applications by virtue of their high power to weight ratio and the ability to apply very large force and torque. However, the dynamics of hydraulic systems are highly nonlinear [10]. Aside from the nonlinear of the electro-hydraulic actuators, they also have large extent of model uncertainties and uncertain nonlinearities such as the frictions. Moreover, the robotic exoskeleton and the actuators are coupled with each other, and there are uncertainties, un-modeled dynamics and disturbance [11]. The design of upper-limb exoskeleton is one of the most challenging tasks to operate under various complex environmental conditions.

The conventional proportional integration derivative (PID) controller is widely used because of its simple control structure, ease of design, and low cost [12]. However, the PID based controller are designed without considering the coupling, their performance is normally affected by the

disturbance inputs and external disturbances. To attenuate disturbance and improve performance of the exoskeleton systems, several researchers have concentrated on exploring diverse control techniques, such as sliding mode control (SMC), and fuzzy logic control, active disturbance rejection control(ADRC) and so on. Teng et al., proposed a method combining PID control, sliding mode control, and fuzzy logic control, PD-based fuzzy sliding mode control, is developed to deal with unmodeled dynamics and external disturbances in the human-exoskeleton system [13]. Sun et al., presented a reduced adaptive fuzzy system together with a compensation term [14]. Compared to traditional approaches, the proposed fuzzy control approach can reduce possible chattering phenomena and achieve better control performance. Torabi. M et al., designed adaptive SMC scheme to provide robustness against disturbances with unknown bounds [15].

Apart from model-based controllers depend on accurate knowledge of the system, non-model based methods exist such as ADRC. To actively estimate and compensate for disturbance, some ADRC techniques are further studied. The original ADRC was first proposed by Han in 1998. As the core of the ADRC, the nonlinear extended state observer (ESO) can estimate and compensate for the total disturbance in the system to achieve stronger anti disturbance performance [16]. The ADRC technique based on ESO, has been successfully used in robot application [17]. Huang et al. presented an optimized linear active disturbance rejection controller to improve the response rapidity and anti-interference ability of a pneumatic servo system [18]. Pawar S. N. et al. designed a modified reduced order ESO based ADRC to estimate the lumped disturbance actively as an extended state and compensate its effect by adding it to the control [19]. As an alternative, the scheme avoids the complete knowledge of the dynamics, simplifying the model to a set of disturbed systems where the set of disturbances includes external disturbance inputs, internal perturbation and non-mode dynamics, which are on-line estimated for subsequent proper cancellation [20, 21]. Since the stability condition of the closed-loop system is expressed in the form of an explicit set of parameters, the tuning law of the ADRC can be intuitively obtained and described in engineering practice.

The goal is to design a controller for upper-limb exoskeleton actuated by hydraulic that can provide good position tracking to compensate for the robot's dynamics and can provide comfortable human-machine interaction. The main contributions of this paper are listed as follows. First, the ADRC was proposed to improve the performance of the upper-limb exoskeleton through the disturbance estimating and finite-time convergence. Second, the effectiveness of the proposed method is verified by numerical simulation through comparing with the PID and ADRC method. This paper is organized as follows. The next section presents the 2-DOF upper-limb exoskeleton kinematic model and the EHSS model. While the ADRC method for position control is presented in Section 3. To demonstrate the performance of the proposed method, the simulation results are presented in Section 4. The main content is summarized and key point of future work are discussed in the final section.

2. System modeling

2.1. Modeling of upper-limb exoskeleton

The exoskeleton is a typical human-robot collaboration system. The control systems of exoskeleton are different from the traditional robots, because the human operator is not the commander of the system, but also a part of the control loop. Hence, the human operator mainly makes the decisions, then the exoskeleton implements the tasks. A model of a 2-DOF upper-limb exoskeleton consisting of the load, the exoskeleton and an operator is shown in Fig. 1. The upper-limb exoskeleton has 2 DOFs, with the shoulder joint and elbow joint actuated and capable of following the rotations of the corresponding joints of the operator.

Without loss of generality, the dynamic equation of the upper-limb exoskeleton robot can be express as follows:

$$\mathbf{T} + \mathbf{T_d} = \big(\mathbf{M}(q) + \mathbf{\Delta M}(q)\big)\ddot{\mathbf{q}} + \big(\mathbf{C}(q,\dot{q}) + \mathbf{\Delta C}(q,\dot{q})\big) + \big(\mathbf{G}(q) + \mathbf{\Delta G}(q)\big), \tag{1}$$

where $\mathbf{T} = [T_1, T_2]^T \in R^{2\times1}$ is a vector of actuator joint torque; $\mathbf{q} = [q_1, q_2]^T \in R^{2\times1}$ is a vector of exoskeleton angles for revolute joints; $\dot{\mathbf{q}}$ and $\ddot{\mathbf{q}}$ are the joint velocities and accelerations respectively. $\mathbf{T}_d$ is the total disturbances of the system. Meanwhile, $\mathbf{M}(q)$ is the inertia matrix, $\mathbf{C}(q,\dot{q})$ is the centripetal matrix, and $\mathbf{G}(q)$ is the gravity torque, respectively. $\mathbf{\Delta M}(q)$, $\mathbf{\Delta C}(q,\dot{q})$ and $\mathbf{\Delta G}(q)$ denote the uncertainty of the robot system. The specific expression of the matrices $\mathbf{M}$, $\mathbf{C}$ and $\mathbf{G}$ can be described as:

$$\mathbf{M} = \begin{bmatrix} M_{11} & M_{12} \\ M_{21} & M_{22} \end{bmatrix}, \quad \mathbf{C} = \begin{bmatrix} C_1 \\ C_2 \end{bmatrix}, \quad \mathbf{G} = \begin{bmatrix} G_1 \\ G_2 \end{bmatrix}, \tag{2}$$

where

$$\begin{cases} M_{11} = I_1 + I_2 + m_1 {l_{G1}}^2 + m_2\left({l_1}^2 + {l_{G2}}^2\right) + 2m_2 l_1 l_{G2}\cos q_2, \\ M_{12} = I_2 + m_2 {l_{G2}}^2 + m_2 l_1 l_{G2}\cos q_2, \\ M_{21} = I_2 + m_2 {l_{G2}}^2 + m_2 l_1 l_{G2}\cos q_2, \\ M_{22} = I_2 + m_2 {l_{G2}}^2, \end{cases}$$

$$\begin{cases} C_1 = -(m_2 + m_l) l_1 l_{G2}(2q_1 q_2 + \dot{q}_2^2)\sin(q_2) - (m_2 + m_l) l_1 l_{G2}\dot{q}_1^2 \sin(q_2), \\ C_2 = (m_2 + m_l) l_1 l_{G2}\dot{q}_1^2 \sin(q_2), \end{cases}$$

$$\begin{cases} G_1 = (m_2 + m_l) g l_{G2}\sin(q_1 + q_2) + m_1 g l_{G1}\sin(q_1) + (m_2 + m_l) g l_1 \sin(q_1), \\ G_2 = (m_2 + m_l) g l_{G2}\sin(q_1 + q_2), \end{cases}$$

where m_1 is the mass of the robotic upper arm, m_2 is the mass of the robotic forearm, l_1 is the length of the robotic upper arm, m_l is the mass of external load, l_2 is the length of the robotic forearm, l_{G1} is the position of the center of the robotic upper arm, l_{G2} is the position of the center of the robotic forearm, I_1 is the inertia of the robotic upper arm and I_2 is the inertia of the robotic forearm.

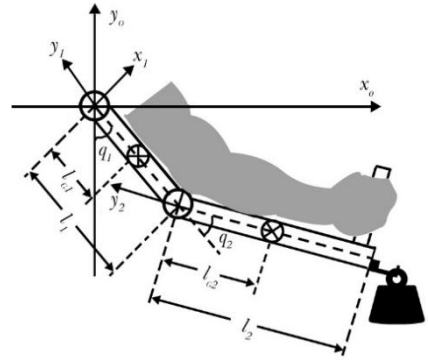

Fig. 1. Model of a 2-DOF upper-limb exoskeleton

Based on the dynamics model of robotic exoskeleton shown by Eq. (1), The system should be decoupled, and matrix $\mathbf{M}(q) + \mathbf{\Delta M}(q)$ can be approximated as $\mathbf{M}(q)$. Assumption:

$$\boldsymbol{\lambda}(q,\dot{q},t) = \mathbf{T}_d - \mathbf{\Delta C}(q,\dot{q}) - \mathbf{\Delta G}(q). \tag{3}$$

The mathematical model of robotic exoskeleton can be expressed as below:

$$\mathbf{M}(q)\ddot{\mathbf{q}} + \mathbf{C}(q,\dot{q}) + \mathbf{G}(q) = \mathbf{T} + \boldsymbol{\lambda}(q,\dot{q},t). \tag{4}$$

The inertia matrix is symmetric positive definite, Eq. (4) can be rewritten as:

$$\ddot{\mathbf{q}} = \boldsymbol{\tau} + \mathbf{f}, \tag{5}$$

where$\boldsymbol{\tau} = \mathbf{M^{-1}}(q)\mathbf{T}$, $\mathbf{f} = \mathbf{M^{-1}}(q)(\boldsymbol{\lambda}(q, \dot{q}, t) - \mathbf{C}(q, \dot{q}) - \mathbf{G}(q))$. $\mathbf{f} = [f_1, f_2]^T$ is the total disturbance of the system, including system error, external disturbance and couple term. $\ddot{\mathbf{q}} = [\ddot{q}_1, \ddot{q}_2]^T$ is the acceleration of the revolute joints.

2.2. Modeling of the electro-hydraulic servo system

The structure of EHSS is shown in Fig. 2. In many EHSS applications, valve dynamics is much faster than other parts of the system. Therefore, valve dynamics can be neglected, we assumed that the servo valve as a proportional block, by following approximation:

$$x_v = k_c i, \tag{6}$$

where k_c is a positive electrical constant, and i is the input current.

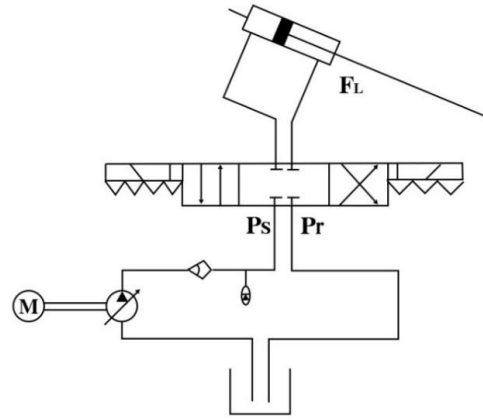

Fig. 2. The structure of EHSS

By applying the continuity law to each actuator chamber, the external leakage of EHSS is extremely small and can be neglected. The flow equation of actuator's valve is described as:

$$\begin{cases} Q_1 = C_d w \sqrt{\dfrac{2}{\rho}} x_v \left[s(x_v)\sqrt{P_s - P_1} + s(-x_v)\sqrt{P_1 - P_r} \right], \\ Q_2 = C_d w \sqrt{\dfrac{2}{\rho}} x_v \left[s(x_v)\sqrt{P_2 - P_r} + s(-x_v)\sqrt{P_s - P_1} \right], \end{cases} \tag{7}$$

where Q_1 is the supplied flow rate to the forward chamber; Q_2 is return flow rate of the return chamber. C_d is the discharge coefficient; w is the spool valve area gradient; ρ is the density of hydraulic oil; P_s is the supply pressure of the fluid; P_r is the return pressure; P_1 is the head-side pressure; P_2 is the rod-side pressure; $S(x_v)$ is defined as:

$$s(x_v) = \begin{cases} 1, & x_v \geq 0, \\ 0, & x_v < 0. \end{cases} \tag{8}$$

The pressure dynamics in actuator chambers can be described as:

$$\begin{cases} \dot{P}_1 = \dfrac{\beta}{V_1}\left[-A_{p1}v_p - C_t P_L + Q_1\right], \\ \dot{P}_2 = \dfrac{\beta}{V_2}\left[A_{p1}v_p + C_t P_L - Q_2\right], \end{cases} \tag{9}$$

where V_1, V_2 are the control volumes of the actuator chambers; β is the effective bulk modulus of the system; C_t is the coefficient of the total internal leakage of the actuator due to the pressure; $P_L = P_1 - P_2$ is the load pressure of the dynamic actuator. The actuated force can be express as:

$$\begin{cases} F_L = P_1 A_{p1} - P_2 A_{p2}, \\ A_{p1} = \dfrac{\pi D_1^2}{4}, \\ A_{p2} = \dfrac{\pi (D_1^2 - D_2^2)}{4}, \end{cases} \tag{10}$$

where A_{p1} is the head-side area; A_{p2} is the rod-side area. D_1 is the bore diameter; D_2 is the rod diameter. As the rod diameter is small compared to the bore diameter, the A_{p2} can be simplified as:

$$A_{p2} = \frac{\pi (D_1^2 - D_2^2)}{4} \approx \frac{\pi D_1^2}{4} = A_{p1}. \tag{11}$$

The EHSS driving torque T can be express as:

$$T = (P_1 - P_2) A_{p1} H, \tag{12}$$

where H is arm of torque.

For the 2-DOF upper-limb exoskeleton, two sets of EHSS generate the force to drive the robotic shoulder and arm respectively:

$$\mathbf{T} = \begin{bmatrix} T_1 \\ T_2 \end{bmatrix} = \begin{bmatrix} (P_{11} - P_{21}) A_{p1} H_1 \\ (P_{12} - P_{22}) A_{p1} H_2 \end{bmatrix}, \tag{13}$$

where T_1 and T_2 are the actuator torques of shoulder joint and elbow joint. P_{11} and P_{21} are the head-side pressure and rod-side pressure of shoulder joint. P_{12} and P_{22} are the head-side pressure and rod-side pressure of elbow joint. H_1 and H_2 are the arms of force for the robotic shoulder and elbow. Based on the geometry of robotic exoskeleton, the H_1 and H_2 can be calculated as:

$$\begin{cases} H_1 = \dfrac{ab\sin(q_1)}{\sqrt{a^2 + b^2 - 2ab\sin(q_1)}}, \\ H_2 = \dfrac{-(l_1 - c)d\cos(q_2)}{\sqrt{(l_1 - c)^2 + d^2 + 2(l_1 - c)d\cos(q_2)}}, \end{cases} \tag{14}$$

where a, b, c and d are the geometric length of the upper limb exoskeleton. Fig. 3 provides the design geometry of the exoskeleton hydraulic cylinder.

The parameters of Electro-hydraulic Servo system are used in Table 1.

3. Control strategy design for upper-limb exoskeleton

The purpose of our upper-limb exoskeleton design is to evaluate the position tracking

performance. To implement this goal, the desired position should be acquired. In this system, the desired angles for revolute joints for the test purposes are sinusoidal signals at a sampling frequency of $f = 1000$ Hz:

$$\begin{cases} q_{d1} = \dfrac{\pi}{6}\sin(2\pi f t), \\ q_{d2} = \dfrac{\pi}{4}\sin(2\pi f t), \end{cases} \quad 0 \le t \le 3. \tag{15}$$

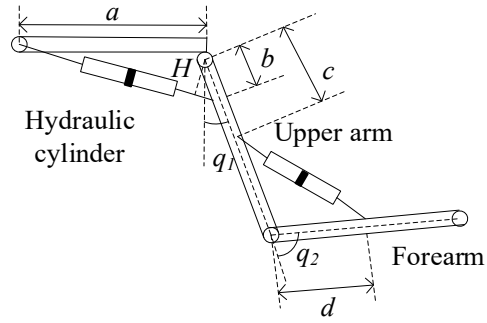

Fig. 3. The design geometry of the exoskeleton hydraulic cylinder

Table 1. Parameters of EHSS

Parameter	Representation	Value
A_{p1}	Head-side area	1.77×10^{-4} m^2
A_{p2}	Rod-side area	1.57×10^{-4} m^2
D_1	Bore diameter	0.015 m^2
D_2	Rod diameter	0.0075 m^2
P_r	Return pressure	5×10^4 Pa
P_s	Supply pressure of the fluid	2×10^6 Pa
ρ	Density of hydraulic oil	830 kg m^3
w	Spool valve area gradient	9.59×10^{-3} m^2
β	Effective bulk modulus of the system	2×10^7 Pa
C_d	Discharge coefficient	0.61
C_t	Coefficient of the total internal leakage	8×10^{-12} M^{5}N^{-1}s^{-1}
k_c	Positive electrical constant	1.38×10^{-4} m^{3}s^{-1}Pa^{-1}
V_1	Volume of the actuator chamber	1.4×10^{-4} m^3
V_2	Volume of the actuator chamber	1.4×10^{-4} m^3
l_1	Length of the robotic upper arm	0.45 m
l_2	Length of the robotic forearm	0.5 m

3.1. Design PID controller for upper-limb exoskeleton

The conventional PID controller is widely adopt due to its simple structure and its gains can be easily tuned. The fixed PID controller of the hydraulically actuated exoskeleton system is shown in Fig. 4, and can be constructed as follows:

$$\begin{cases} i_1(t) = K_{p1}e_1(t) + K_{i1}{e_1}^{-1}(t) + K_{d1}{e_1}'(t), \\ i_2(t) = K_{p2}e_2(t) + K_{i2}{e_2}^{-1}(t) + K_{d2}{e_2}'(t), \end{cases} \tag{16}$$

where $K_{p1}(K_{p2})$, $K_{i1}(K_{i2})$ and $K_{d1}(K_{d2})$ are proportional, integration and differential gains respectively. Moreover, $e_1(t) = q_{d1}(t) - q_1(t)$ and $e_2(t) = q_{d2}(t) - q_2(t)$ are the errors between the desired positions and actual positions.

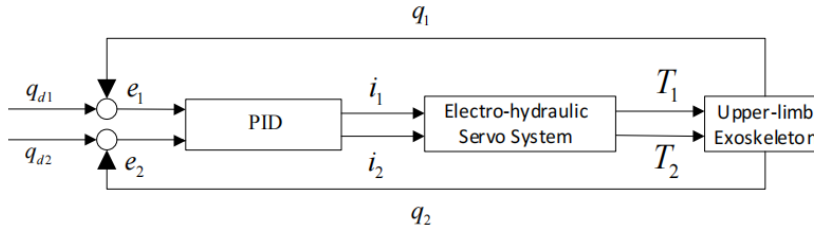

Fig. 4. Block diagram of PID controller

3.2. Design ADRC for upper-limb exoskeleton

The ADRC method adopt nonlinear function, resulting in difficult analysis and parameter setting complex. Therefore, ADRC is designed based on the dynamic of robotic exoskeleton. In this paper, the dynamics model of the exoskeleton leg is multi-input and multi-output (MIMO) system. The Block diagram of ADRC controller is shown in Fig. 5. After system is decoupled, ADRC can be designed to control each joint respectively. Eq. (5) can be split into two independent equations for the shoulder and elbow joint as follow:

$$\begin{cases} \ddot{q}_1 = \tau_1 + f_1, \\ \ddot{q}_2 = \tau_2 + f_2. \end{cases} \tag{17}$$

The ADRC controller consist three main parts, i.e., the tracking differentiator (TD) to provide derivative of the input signal, the extend state observer (ESO) to estimate the states and the disturbances and the nonlinear feedback to generate the control signal. TD is used to generate the arranged transition process and extract the input signal's differential of each order. The tracking differentiator is designed in the form of:

$$\begin{cases} \dot{v}_1 = v_2, \\ \dot{v}_2 = k_1(v_1 - q_{d1}) - k_2 v_2, \end{cases} \quad \begin{cases} \dot{v}_3 = v_4, \\ \dot{v}_4 = k_1(v_3 - q_{d2}) - k_2 v_4, \end{cases} \tag{18}$$

where q_{d1} and q_{d2} are desired angles, k_1 and k_2 are the observer gains to ensure convergence of the error. ESO is designed to estimate and compensation total disturbances of hydraulically actuated exoskeleton system. Two extended state observers can be obtained as follows:

$$\begin{cases} \dot{z}_1 = z_2 + \beta_{11} e_1, \\ \dot{z}_2 = z_3 + \beta_{12} e_1 + b_0 i_1, \\ \dot{z}_3 = \beta_{13} e_1, \end{cases} \quad \begin{cases} \dot{z}_4 = z_5 + \beta_{21} e_2, \\ \dot{z}_5 = z_6 + \beta_{22} e_2 + b_1 i_2, \\ \dot{z}_6 = \beta_{23} e_2, \end{cases} \tag{19}$$

where β_{11}, β_{12}, β_{13} and β_{21}, β_{22}, β_{23} are the observer gains. The observations error are defined as $e_1 = z_1 - q_1$, $e_2 = z_4 - q_2$. For the purpose of tuning simplification, all the observer poles are placed at $-\omega_0$. The observer gains can be determined according to the characteristic polynomial [22]:

$$\begin{aligned} s^3 + \beta_{11} s^2 + \beta_{12} s + \beta_{13} &= (s + w_0)^3, \\ s^3 + \beta_{21} s^2 + \beta_{22} s + \beta_{23} &= (s + w_0)^3, \end{aligned} \tag{20}$$

where ω_0 is the bandwidth of observer and the gain vector can be expressed as follows: $\beta_{11} = 3\omega_0$, $\beta_{12} = 3{\omega_0}^2$, $\beta_{13} = \omega_0^3$ and $\beta_{21} = 3\omega_0$, $\beta_{22} = 3{\omega_0}^2$, $\beta_{23} = \omega_0^3$. In this paper, the bandwidth of two observers is defined as the same values of $-\omega_0$. The bandwidth of feedback

controller is defined as $\omega_c = \frac{1}{3}\omega_0$. Finally, the feedback control law in the proposed control can be written as follows:

$$\begin{cases} u_1 = k_{p1}(z_1 - v_1) + k_{d1}(z_2 - v_2), \\ i_1 = u_1 - \dfrac{z_3}{b_0}, \\ u_2 = k_{p2}(z_4 - v_3) + k_{d2}(z_5 - v_4), \\ i_2 = u_2 - \dfrac{z_6}{b_1}, \end{cases} \tag{21}$$

where k_{p1}, k_{p2} and k_{d1}, k_{d2} are the proportional and differential gains, respectively.

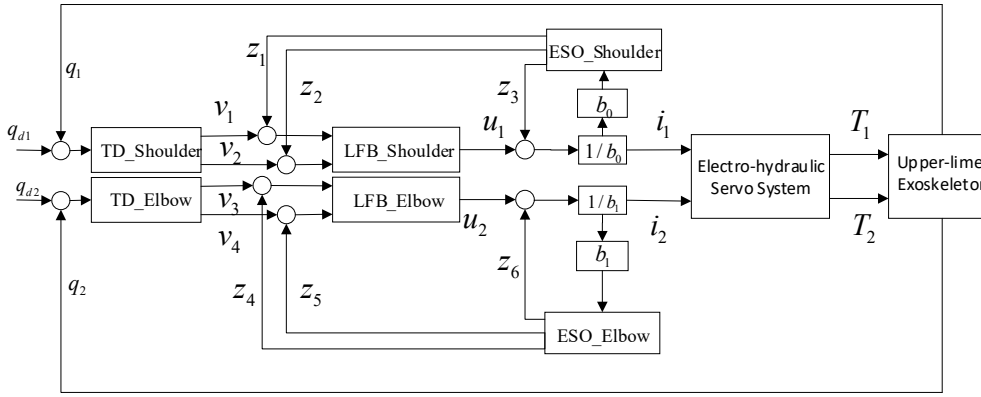

Fig. 5. Block diagram of ADRC controller

4. Simulation results

4.1. Selection of system parameters

The objectives of this section are to compare the tracking performance of PID control approach and the ADRC strategy. There are two ESOs to estimate existing disturbance for the shoulder joint and the elbow joint respectively. The parameters of the EHSS and the upper-limb exoskeleton are listed in Table 1. Two simulations are carried out, in MATLAB, by using PID control strategy and the ADRC. The parameters of ADRC are shown in Table 2, b_0 and b_1 are the amplification coefficients of i_1 and i_2. w_0 is the bandwidth of observer, and the selection of its value affect the tracking effect.

Table 2. Parameters for ADRC

Symbol	Value	Symbol	Value
b_0	1	b_1	4
w_0	1200	β_{21}	3600
β_{11}	3600	β_{22}	4.32×10^6
β_{12}	4.32×10^6	β_{23}	1.728×10^9
β_{13}	1.728×10^9	k_{p2}	160000
k_{p1}	160000	k_{d2}	800
k_{d1}	800		

Fig. 6 shows the tracking error of each joint with different w_0 in proposed ADRC. As seen in the figure, the error decrease as the value of w_0 increases, the larger the value of w_0 is, the faster the errors converge.

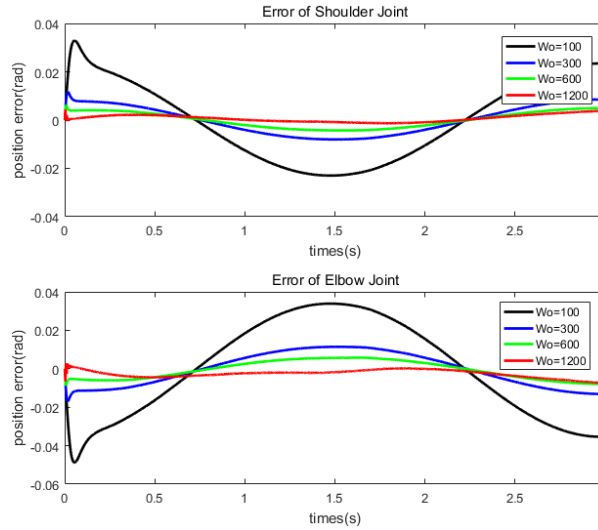

Fig. 6. Tracking error with different w_0 in proposed ADRC

4.2. Comparisons of the conventional PID controller and ADRC controller

The system simulations are carried out, in MATLAB (Version R2016a), by using PID control strategy and ADRC approach presented in respectively. The parameters of the controllers are chosen using Ziegler and Nichols method [23]. Then, the optimum parameters for the PID controller can be provided as $K_{p1} = 240$, $K_{i1} = 40$, $K_{d1} = 180$ and $K_{p2} = 200$, $K_{i2} = 80$, $K_{d2} = 120$. The external disturbance is generated by a sinusoidal signal as follows:

$$f_1 = f_2 = 0.01\sin(10\pi t). \tag{22}$$

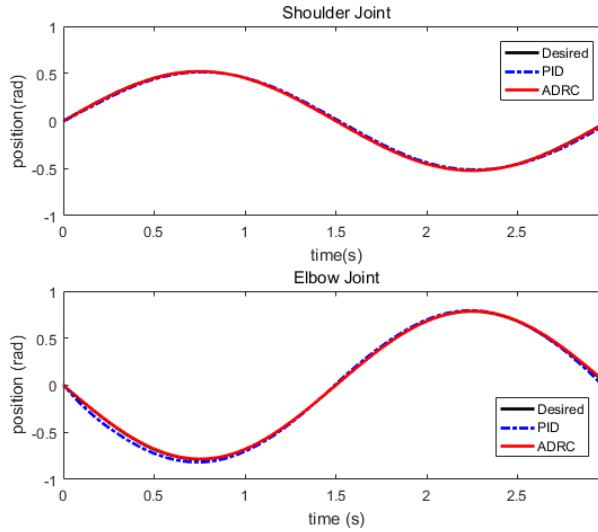

Fig. 7. Trajectory tracking comparison of PID and LADRC

Performances of the conventional PD controller and ADRC method for position trajectory control are compared next. Figs. 7, 8 show trajectory tracking, position errors for each joint. As shown in the Fig. 7, The trajectories produced by the PID controller is depicted in red color, then ADRC is depicted in blue color, and the desired angle is depicted in black color. The performance

of ADRC method is better compared to the conventional PID control. Fig. 8 shows the trajectory tracking error of the shoulder joint and the elbow joint respectively. It is seen that the deviations occur from the desired trajectory and ADRC controller produces better results than the conventional PID controller. The ADRC controller possess 3 ms lag, which is smaller than 11ms lag for the PID controller.

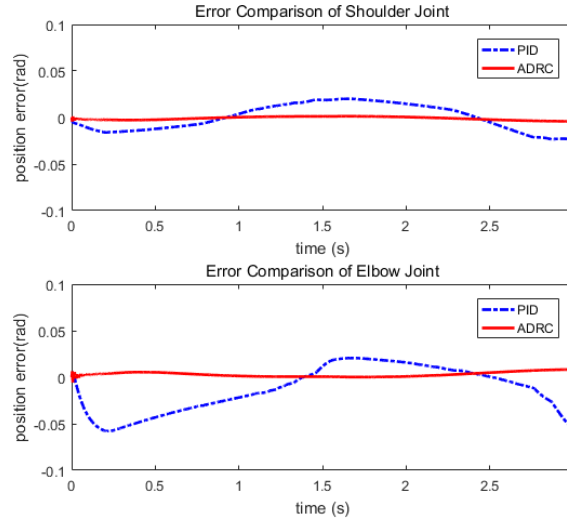

Fig. 8. Tracking error comparison of PID and ADRC

To evaluate the performance of the general PID control approach and the proposed method, the tracking errors are compared. The tracking performances are indicated by root-mean-square (RMS) error [12]:

$$RMS = \sqrt{\frac{1}{n}\sum_{1}^{n}(q - q_d)^2}. \tag{23}$$

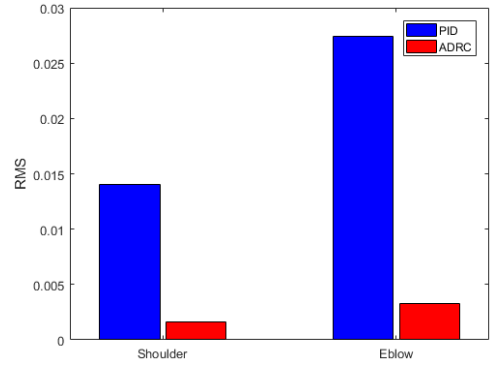

Fig. 9. RMS comparison between PID and ADRC

Fig. 9 provides the RMS errors of the human-machine position. From Fig. 9, both of the tracking errors of shoulder joint and elbow joint under the ADRC approach are smaller than those under the conventional PID control strategy. It is obviously to see that the proposed ADRC method is better than PID control with its robustness to external disturbance or un-modeled system dynamic, and it will be easy to implement.

5. Conclusions

The ADRC strategy for 2-DOF upper-limb exoskeleton, under the actuation of hydraulic, was explored in this paper. Considering the unavailability of precise model parameters and the uncertain disturbances in upper-limb exoskeleton actuated by EHSS. The proposed control strategies not only reduce the influence of unknown disturbances and eliminates the dependence on accurate model parameters, but also improve the tracking accuracy of the exoskeleton system and make the error converge quickly. The simulation results validate the effectiveness of the proposed method. The limitation of our approach is tuning the ADRC parameters automatically. In the future, the combination of ADRC with other model free tuning techniques will be investigated to reduce this limitation. It is proposed for the further development to investigate the robustness of ADRC for the external load uncertainty and motion velocity change. Moreover, Future work will include applying different types of other path tracking trajectories.

Acknowledgements

This work was supported by Key Research and Development Plan of Hubei Province (2021BGD013), Hubei University of Technology Ph.D. Research Startup Fund Project (BSQD2020014) and Science and Technology Research Program of Hubei Provincial Department of Education (T201805).

Data availability

The datasets generated during and/or analyzed during the current study are available from the corresponding author on reasonable request.

Author contributions

Jing Tang: application of statistical, mathematical and computational, to synthesize study data. conducting a research and investigation process, specifically performing the experiments and data collection. Jiaxun Cao: Preparation and presentation of the published work by those from the original research group. Minghu Wu: management and coordination responsibility for the research activity planning and execution. Lun Zhao: preparation and presentation of the published work, specifically data presentation. Fan Zhang: software development; designing computer programs; implementation of the computer code and supporting algorithms.

Conflict of interest

The authors declare that they have no conflict of interest.

References

[1] D. Calafiore, F. Negrini, N. Tottoli, F. Ferraro, O. Ozyemisci-Taskiran, and A. de Sire, "Efficacy of robotic exoskeleton for gait rehabilitation in patients with subacute stroke: a systematic review," *European Journal of Physical and Rehabilitation Medicine*, Vol. 58, No. 1, pp. 1–8, Mar. 2022, https://doi.org/10.23736/s1973-9087.21.06846-5

[2] A. Rodríguez-Fernández, J. Lobo-Prat, and J. M. Font-Llagunes, "Systematic review on wearable lower-limb exoskeletons for gait training in neuromuscular impairments," *Journal of NeuroEngineering and Rehabilitation*, Vol. 18, No. 1, pp. 1–21, Dec. 2021, https://doi.org/10.1186/s12984-021-00815-5

[3] C. Kandilakis and E. Sasso-Lance, "Exoskeletons for personal use after spinal cord injury," *Archives of Physical Medicine and Rehabilitation*, Vol. 102, No. 2, pp. 331–337, Feb. 2021, https://doi.org/10.1016/j.apmr.2019.05.028

[4] J. Kim et al., "Reducing the metabolic rate of walking and running with a versatile, portable exosuit," *Science*, Vol. 365, No. 6454, pp. 668–672, Aug. 2019, https://doi.org/10.1126/science.aav7536

[5] Z. Wang et al., "Study on the control method of knee joint human-exoskeleton interactive system," *Sensors*, Vol. 22, No. 3, p. 1040, Jan. 2022, https://doi.org/10.3390/s22031040

[6] Z. Li, B. Huang, Z. Ye, M. Deng, and C. Yang, "Physical human-robot interaction of a robotic exoskeleton by admittance control," *IEEE Transactions on Industrial Electronics*, Vol. 65, No. 12, pp. 9614–9624, Dec. 2018, https://doi.org/10.1109/tie.2018.2821649

[7] W. Cao et al., "A lower limb exoskeleton with rigid and soft structure for loaded walking assistance," *IEEE Robotics and Automation Letters*, Vol. 7, No. 1, pp. 454–461, Jan. 2022, https://doi.org/10.1109/lra.2021.3125723

[8] X. Zhang, G. Wang, P. Yuan, H. Xu, and Y. Hou, "A control strategy for maintaining gait stability and reducing body-exoskeleton interference force in load-carrying exoskeleton," *Journal of Intelligent and Robotic Systems*, Vol. 97, No. 2, pp. 287–298, Feb. 2020, https://doi.org/10.1007/s10846-019-01043-9

[9] N. Zhou, Y. Liu, Q. Song, and D. Wu, "A compatible design of a passive exoskeleton to reduce the body-exoskeleton interaction force," *Machines*, Vol. 10, No. 5, p. 371, May 2022, https://doi.org/10.3390/machines10050371

[10] Song, Lee, Park, and Baek, "Design and performance of nonlinear control for an electro-hydraulic actuator considering a wearable robot," *Processes*, Vol. 7, No. 6, p. 389, Jun. 2019, https://doi.org/10.3390/pr7060389

[11] C. Yang, Q. Huang, and J. Han, "Decoupling control for spatial six-degree-of-freedom electro-hydraulic parallel robot," *Robotics and Computer-Integrated Manufacturing*, Vol. 28, No. 1, | pp. 14–23, Feb. 2012, https://doi.org/10.1016/j.rcim.2011.06.002

[12] J. Tang, J. Zheng, and Y. Wang, "Direct force control of upper-limb exoskeleton based on fuzzy adaptive algorithm," *Journal of Vibroengineering*, Vol. 20, No. 1, pp. 636–650, Feb. 2018, https://doi.org/10.21595/jve.2017.18610

[13] L. Teng, M. A. Gull, and S. Bai, "PD-based fuzzy sliding mode control of a wheelchair exoskeleton robot," *IEEE/ASME Transactions on Mechatronics*, Vol. 25, No. 5, pp. 2546–2555, Oct. 2020, https://doi.org/10.1109/tmech.2020.2983520

[14] W. Sun, J.-W. Lin, S.-F. Su, N. Wang, and M. J. Er, "Reduced adaptive fuzzy decoupling control for lower limb exoskeleton," *IEEE Transactions on Cybernetics*, Vol. 51, No. 3, pp. 1099–1109, Mar. 2021, https://doi.org/10.1109/tcyb.2020.2972582

[15] M. Torabi, M. Sharifi, and G. Vossoughi, "Robust adaptive sliding mode admittance control of exoskeleton rehabilitation robots," *Scientia Iranica*, Oct. 2017, https://doi.org/10.24200/sci.2017.4512

[16] C. Dai, J. Yang, Z. Wang, and S. Li, "Universal active disturbance rejection control for non-linear systems with multiple disturbances via a high-order sliding mode observer," *IET Control Theory and Applications*, Vol. 11, No. 8, pp. 1194–1204, May 2017, https://doi.org/10.1049/iet-cta.2016.0709

[17] J. Li, Y. Xia, X. Qi, and P. Zhao, "Robust absolute stability analysis for interval nonlinear active disturbance rejection based control system," *ISA Transactions*, Vol. 69, pp. 122–130, Jul. 2017, https://doi.org/10.1016/j.isatra.2017.04.017

[18] Y. Huang and J. R. Wang, "Optimized linear active disturbance rejection controller design for hydraulic turbine governing system," *Journal of System Simulation*, Vol. 28, No. 12, pp. 3033–3040, 2016.

[19] S. N. Pawar, R. H. Chile, and B. M. Patre, "Modified reduced order observer based linear active disturbance rejection control for TITO systems," *ISA Transactions*, Vol. 71, pp. 480–494, Nov. 2017, https://doi.org/10.1016/j.isatra.2017.07.026

[20] L. Sun, Q. Hua, D. Li, L. Pan, Y. Xue, and K. Y. Lee, "Direct energy balance based active disturbance rejection control for coal-fired power plant," *ISA Transactions*, Vol. 70, pp. 486–493, Sep. 2017, https://doi.org/10.1016/j.isatra.2017.06.003

[21] L. Zhao, B. Zhang, H. Yang, and Q. Li, "Optimized linear active disturbance rejection control for pneumatic servo systems via least squares support vector machine," *Neurocomputing*, Vol. 242, pp. 178–186, Jun. 2017, https://doi.org/10.1016/j.neucom.2017.02.069

[22] Qing Zheng, Lili Dong, Dae Hui Lee, and Zhiqiang Gao, "Active disturbance rejection control for MEMS gyroscopes," in *2008 American Control Conference (ACC '08)*, pp. 4425–4430, Jun. 2008, https://doi.org/10.1109/acc.2008.4587191

[23] J. G. Ziegler and N. B. Nichols, "Optimum settings for automatic controllers," *Journal of Dynamic Systems, Measurement, and Control*, Vol. 115, No. 2B, pp. 220–222, Jun. 1993, https://doi.org/10.1115/1.2899060

Jing Tang received B.Sc. degree in 2007 and M.E degree in 2010 from Chongqing University of Posts and Telecommunications of China. She received Ph.D. from Wuhan University of Technology in 2019. She is a lecturer at School of electrical and electronic engineering in Hubei University of Technology, Wuhan, China. She is a member of the Project-National Key R&D Program of China "The study on Load-bearing and Moving Support Exoskeleton Robot Key Technology and Typical Application", where she carried out research concerning control of the human-robot coordinated of exoskeletons system and human locomotion intention recognition. Her research interests focus on pattern recognition, intelligent control and design wearable exoskeleton to understand more of human ambulation.

Jiaxun Cao received M.E degree in 2017 from Jinan University. He studies for a master's degree in Hubei University of Technology.

Minghu Wu received the B.S. degree in electronic information engineering from the Communication University of China, Beijing, China, in 1998, the M.S. degree in communication information system from the Huazhong University of Science and Technology, Wuhan, China, in 2002, and the Ph.D. degree from the Nanjing University of Posts and Telecommunications, Nanjing, China, in 2013. He is currently a Professor with the Hubei University of Technology. His major research interests include communication signal processing and video coding.

Lun Zhao received M.E degree in 2017 from Wuchang Institute of Technology. He studies for a master's degree in Hubei University of Technology.

Fan Zhang received the telecommunication engineering degree and the Ph.D. degree in radio physics from Wuhan University, Wuhan, China in 2009 and 2014, respectively. She is currently with the School of Electrical and Electronic Engineering, Hubei University of Technology, Wuhan, China. Her current research interests include electromagnetic theory and its application, radar imaging and signal processing.